Parametric FEA Study of Burst Pressure of Cylindrical Shell Intersections

L. Xue
MMI Engineering,
11490 Westheimer Road,
Suite 150,
Houston, TX 77077

G. E. O. Widera
Center for Joining and Manufacturing Assembly,
Marquette University,
Milwaukee, WI 53201

Z. Sang
College of Mechanical Engineering,
Nanjing University of Technology,
Nanjing, Jiangsu 210009, P.R. China

*In an earlier paper (2009, "Burst Pressure of Pressurized Cylinders With the Hillside Nozzle," ASME J. Pressure Vessel Technol., **131**(4), p. 041204), an elastic-plastic large deflection analysis method was used to determine the burst pressure and fracture location of hillside cylindrical shell intersections by use of nonlinear finite element analysis. To verify the accuracy of the finite element results, experimental burst tests were carried out by pressurizing test vessels with nozzles to burst. Based on the agreement between the numerical simulations and experimental results of Wang et al. (2009, "Burst Pressure of Pressurized Cylinders With the Hillside Nozzle," ASME J. Pressure Vessel Technol., **131**(4), p. 041204), a parametric study is now carried out. Its purpose is to develop a correlation equation by investigating the relationship between various geometric parameters (d/D, D/T, and t/T) and the burst pressure. Forty-seven configurations, which are deemed to cover most of the practical cases, are chosen to perform this study. In addition, four different materials are employed to verify that the proposed equation can be employed for different materials. The results show that the proposed equation resulting from the parametric analysis can be employed to predict the static burst pressure of cylindrical shell intersections for a wide range of geometric ratios.* [DOI: 10.1115/1.4000731]

1 Introduction

Cylindrical shell intersections are structural elements, which occur often in many industries. The action of mechanical and thermal loads leads to high local stress in the intersection region, thus resulting in stress concentrations there. Additional difficulties can arise due to welding and this region thus becomes the weakest point and the source of failure of the entire structure. When loaded, for example, with internal pressure, the failure of these intersection elements can cause extensive damage, and it is thus important to be able to predict the magnitude of the burst pressure.

Cottam and Gill [1] carried out 11 tests, to rupture, on mild steel cylindrical pressure vessels with flush nozzles. Two cylindrical vessels without nozzles were also tested to establish datum curves for the vessels with nozzles. Rodabaugh [2] summarized 31 available burst test data and failure locations on basic configuration pipe connections. The basic configuration was a pipe connection consisting of a run pipe with a uniform-wall branch pipe; there was no pad or any other type of reinforcement other than that provided by a fillet weld on the outside surface of the intersection. Burst tests were conducted on two cylindrical shell intersections (90 deg intersection and 30 deg lateral) by Sang et al. [3]. Inspection of the metallographic structure and microstructure of the fracture surface in the initiation area showed that the cylinder wall had obvious plastic deformation in the area of the fracture and was representative of a typical ductile fracture. Although there exist data on burst pressure cylindrical shell intersections determined from experiments, data from this approach are limited due to the difficulties and cost associated with fabricating a precise shell intersection, especially with the large number of possible configurations in real world applications. As a result, finite element analysis (FEA) may be used as a more viable tool to estimate the burst pressure. An elastic-plastic failure analysis of thin toroidal shells using large strain, large displacement, elastic-plastic FEA (LS-LD-EP-FEA) was performed by Jones et al. [4]. A comparison between FEA results and test data from the Pressure Vessel Research Council (PVRC) burst disk program was provided by Jones and Holliday [5]. The results showed that the LS-LD-EP-FEA could provide a best-estimate analysis of the burst of a disk, but that the accuracy would depend on the material stress-strain curve. The burst pressure and failure location of DOT-39 refrigerant cylinders were determined by Kissioglu et al. [6] using both experimental burst tests and FEA modeling. Having studied the effect of external corrosion defects by use of a nonlinear numerical model based on the finite element method, Loureiro et al. [7] developed a simple procedure for estimating the burst pressure of corroded pipes. The burst pressures of three pipes, each containing a single internal corrosion pit, was determined by Chouchaoui et al. [8] with a very fine finite element mesh. Błachut and Vu [9] computed the burst pressure of shallow spherical caps and torrispheres loaded by uniform pressure. Bursting was determined using the ABAQUS code with axisymmetric shell elements and defined using plastic strain criteria taken from one-dimensional true stress and strain curves. Results were benchmarked against the experimental data. The use of nonlinear FEA to predict the failure pressure of real corrosion defects was investigated by Cronin [10] using the results from 25 burst tests of pipe sections removed from service due to the presence of such defects. The author concluded that the elastic-plastic FEA provided an accurate prediction of the burst pressure and the failure location for complex-shaped corrosion defects.

From the above review it is seen that the burst pressure and failure location of cylindrical shells can be determined with sufficient accuracy by use of a static finite element analysis. As far as radial cylinder-cylinder intersections are concerned, very little published information is available. In this paper, we present a comprehensive study of the burst pressure of these intersections based on the research performed by Xue [11]. The approach presented by Xue was subsequently employed by Wang et al. [12] in their study of the burst pressure of vessels with hillside nozzles. In their paper, the FEA simulation procedure was validated by comparison with the results from experiments employing test vessels, which were hydraulically pressurized to burst. Based on the agreement between the numerical and experimental results, a parametric analysis is here carried out to determine the influence of geo-

Contributed by the Pressure Vessel and Piping Division of ASME for publication in the JOURNAL OF PRESSURE VESSEL TECHNOLOGY. Manuscript received July 14, 2009; final manuscript received November 21, 2009; published online May 4, 2010. Assoc. Editor: Maher Y. A. Younan.

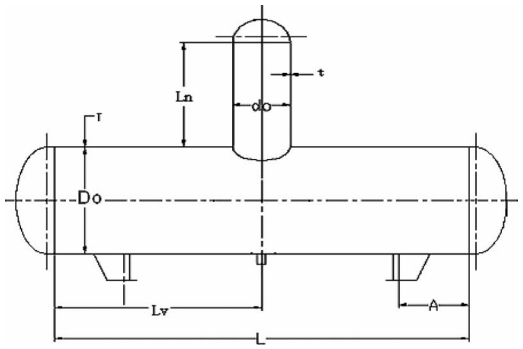

Fig. 1 Schematic of vessel and nozzle

metric parameters (diameter ratio, thickness ratio, and diameter to thickness ratio) on the burst pressure of radial intersections. An empirical formula for this pressure is then developed based on the parametric analysis results.

2 Finite Element Model

A schematic of a cylinder—cylinder intersection (i.e., vessel and nozzle)—is shown in Fig. 1. Static nonlinear (both geometry of deformation and material behavior) finite element analyses of this structure are performed by use of the ANSYS FEA code [13]. Three-dimensional 20-node structural solid elements are used to generate the finite element mesh. Due to the symmetry of the geometry, supports, and loading, only a quarter of the structure is modeled. The guidelines for FEA modeling of cylinder-to-cylinder intersections developed by Widera and Xue [14] are employed to mesh the structure. This leads to a finite element model having 24 elements in the circumferential direction of the nozzle, two elements through the thickness, and 20 elements in the axial direction of the vessel and nozzle prior to reaching the decay distances of the vessel and nozzle ($3.0\sqrt{RT}$ and $3.0\sqrt{rt}$, respectively). The maximum aspect ratio at the intersection area is less than 5. Figure 2 illustrates the finite element mesh of the idealized analysis model, in which the fillet weld at the intersection is not modeled. Reference [12] provides the weld details for the test vessel. This parametric study is carried out on the basis that no defect exists in the weldment so that the burst pressure of cylindrical intersections will not be affected by the weld itself.

Symmetry boundary conditions are employed on the two symmetry planes, the longitudinal ($y=0$) and transverse ($z=0$) planes. The right end of the vessel is fixed in all directions except for the longitudinal (z) one.

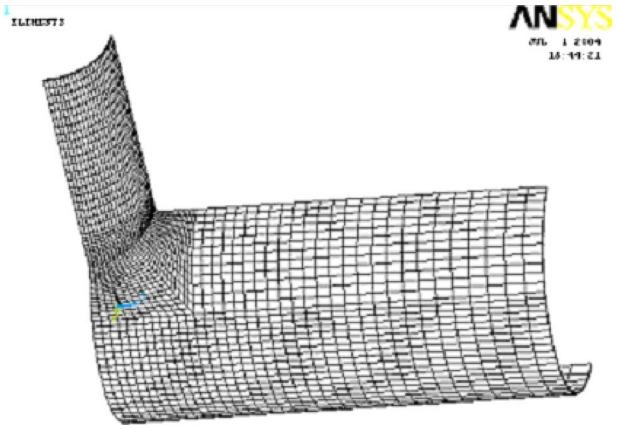

Fig. 2 Finite element model

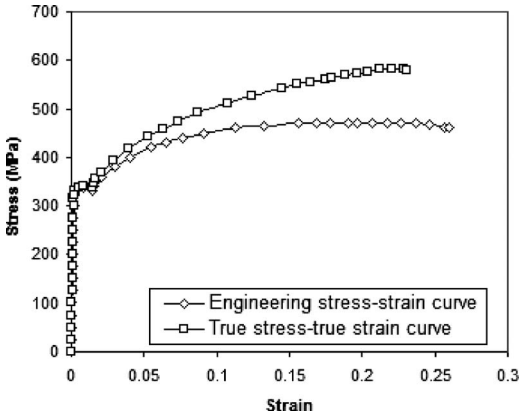

Fig. 3 Stress-strain curve for material 20# (ambient temperature)

The finite element model is subjected to an internal pressure. This pressure is gradually increased in a stepwise fashion, with convergence achieved for each pressure increment. Equivalent axial stresses are imposed as boundary conditions at the ends of the nozzle and vessel to simulate the contained pressure

$$S_{av} = \frac{PD}{4T}\left(\frac{D_i}{D}\right)^2 \tag{1}$$

$$S_{an} = \frac{Pd}{4t}\left(\frac{d_i}{d}\right)^2 \tag{2}$$

Theses stresses are also gradually increased with each load step in proportion to that of the internal pressure.

ANSYS contains two different approaches to solve the present nonlinear problem: the Newton–Raphson method and the arc length method. The latter causes the Newton–Raphson Method to converge along an arc, thereby often preventing divergence. Studies by Xue [11] have shown that while both methods can be employed to predict the burst pressure, the arc length method yields more reliable results.

3 Failure Criterion

In Ref. [11], Xue proposed that a method first used by Jones [5] be employed for the bursting of pressurized cylindrical shells and their intersections. The method was subsequently tested in a study of vessels with hillside nozzles [12]. According to this method, failure occurs when the pressure causes the structure to have a dimensional instability, i.e., unbounded strain occurs for a small increase in pressure. At that time, an increase in volume produces a decrease in pressure and the slope of the pressure—strain curve becomes vanishingly small. The pressure causing this is the burst pressure.

As also shown by Xue [11] and Wang et al. [12], the failure location can be determined by finding the location of the maximum average equivalent plastic strain through the thickness.

4 Material Properties

The material for the vessel and nozzle is 20# (low carbon steel, with properties very similar to A106-80 GrA). Typical partial stress-strain curves of this material are shown in Fig. 3. The multilinear model of the true stress-strain curve is shown in Table 1. Average values of the yield and ultimate tensile strengths are 425 MPa and 472 MPa, respectively.

The ANSYS program was used to carry out the present elastic-plastic analysis, assuming the von Mises yield criterion and a multilinear material hardening law to be valid. The material is assumed to be isotropic and the elastic properties are Poisson's ratio $\upsilon=0.3$ and Young's modulus $E=212$ GPa. The plasticity ra-

Table 1 Multilinear material model for material 20#

Points	1	2	3	4	5	6	7	8	9	10	11	12	13
Strain ($\mu\varepsilon$)	1491	1828	1854	5636	7817	16731	20513	53275	86941	145062	174655	195282	220251
Stress (MPa)	316	325.98	329.6	338.67	340.73	355.93	368.13	443.15	490.98	543.41	562.07	573.16	583

tio governing the convergence of the computations is set at 15% rather than the ANSYS default value of 30%.

5 Lengths of Vessel and Nozzle for Finite Element Models

A convergence study of vessel and nozzle lengths is performed prior to carrying out the parametric study in order to examine the effect of lengths of the vessel and nozzle on the burst pressure prediction. Widera and Wei [15] determined definitive lengths of vessel and nozzle as part of a parametric finite element analysis ($0.333 \le d/D \le 1.0$) to study the stress concentration of shell intersections subjected to internal pressure. In order to determine whether the lengths provided in Ref. [15] have an effect on the burst pressure predictions, even longer models are employed here to carry out a convergence study. Table 2 shows a comparison of the burst pressure for models with $D/T=100$ and $t/T=1$ and shows that the lengths from Ref. [15] are adequate to predict the burst pressure. Therefore, the lengths of the vessel and nozzle for the finite element models shown in Table 3 are employed for the present parametric study.

Table 2 Effect of lengths of vessel and nozzle on burst pressure ($D/T=100$, $t/T=1$)

	$d/D=0.1$	
	$L_v=1.5D$, $L_n=0.5D$	$L_v=2D$, $L_n=D$
P_b	9.72	9.71
	$d/D=0.2$	
	$L_v=1.5D$, $L_n=0.5D$	$L_v=2D$, $L_n=D$
P_b	9.40	9.39
	$d/D=0.333$	
	$L_v=2.5D$, $L_n=D$ [a]	$L_v=3D$, $L_n=1.5D$
P_b	9.03	9.02
	$d/D=0.5$	
	$L_v=2.5D$, $L_n=1.5D$ [a]	$L_v=3D$, $L_n=2D$
P_b	8.68	8.68
	$d/D=0.75$	
	$L_v=2.5D$, $L_n=2D$ [a]	$L_v=3D$, $L_n=2.5D$
P_b	8.08	8.08
	$d/D=0.95$	
	$L_v=3D$, $L_n=2D$ [a]	$L_v=3.5D$, $L_n=2.5D$
P_b	7.54	7.53

[a]From Ref. [15].

Table 3 Lengths of vessel and nozzle for FE models

d/D	L_v	L_n
0.1	$1.5D$	$0.5D$
0.2	$1.5D$	$0.5D$
0.333	$2.5D$	D
0.5	$2.5D$	$1.5D$
0.75	$2.5D$	$2D$
1	$3D$	$2D$

6 Parametric Analysis

Previous studies by the authors [11,12] demonstrated that a nonlinear FEA in conjunction with the arc length method can be employed with sufficient accuracy to predict the burst pressure of cylindrical shell intersections. In order to develop an empirical formula for the burst pressure, the influence of discrete geometric parameters (diameter (d/D), thickness t/T, and diameter to thickness D/T ratios) is now examined. The choice of these parameters is based on previous parametric studies for the determination of stress concentration factors [11,15,16]. It originated from suggestions made by the PVRC Task Group on Large Diameter Shell Intersections. Table 4 lists the chosen geometric parameters. This table covers practical cases of cylindrical intersections. Due to the difficulty of meshing accurately an equal diameter cylinder-cylinder intersection ($d/D=1$) by use of solid elements, a diameter ratio of 0.95 is instead employed in this study. It is to be noted that the parametric study is carried out based on an idealized physical model without a weld or reinforcement at the junction of the cylinders.

In this study the mean diameter D is taken at 100 mm and d, t, and T will be changed as variables. Table 5 shows the FEA predicted burst pressures of 47 cylindrical shell intersection models and the corresponding burst pressures of plain cylindrical vessels using the Barlow equation [2]

$$P_{bv} = \frac{2\sigma_u T}{D} \tag{3}$$

Reference [2] provides five correlation equations for the estimation of burst pressures of pipe connections by a "least squares" fit of 51 test data. It was noted that the failures of all 15 test models occurred in the longitudinal plane. Two of these equations (see Eqs. (4) and (5) below) are employed here to compare with the FEA results since they have higher correlation coefficients (0.845 and 0.841, respectively). The burst pressures from these equations are also provided in Table 5. In several cases, the differences between P_b^{FEA}, and $P_b^{\text{Eq. (4)}}$ and $P_b^{\text{Eq. (5)}}$ are high. This is deemed acceptable since Eqs. (4) and (5) were developed based on limited experimental data and the correlation coefficients are far from one

$$\frac{P_b}{P_{bv}} = 1.786(SCF)^{-0.5370} \tag{4}$$

$$\frac{P_b}{P_{bv}} = 1.06(P^*)^{0.669} \tag{5}$$

Here SCF and P^* are determined from Eqs. (6) and (7), respectively

Table 4 Range of geometric parameters

Number of models	t/T	D/T	d/D
9	0.1, 1, 3	50, 100, 250	0.1
9	0.2, 1, 3	50, 100, 250	0.2
9	0.333, 1, 3	50, 100, 250	0.333
9	0.5, 1, 3	50, 100, 250	0.5
9	0.75, 1, 3	50, 100, 150	0.75
2	1	50, 100	0.95

Table 5 Burst pressures from FEA and empirical formulas

Model	d/D	D/T	t/T	L_v	L_n	$P_{bv}=2\sigma_u T/D$	P_b^{FEA}	$P_b^{\text{Eq. (40)}}$	$P_b^{\text{Eq. (5)}}$
1			0.1			18.88	15.81	17.79	19.12
2		50	1			18.88	19.65	20.14	21.87
3			3			18.88	19.78	20.14	31.54
4			0.1			9.44	8.16	8.33	8.97
5	0.1	100	1	1.5D	0.5D	9.44	9.72	10.07	10.27
6			3			9.44	9.87	10.07	14.82
7			0.1			3.776	3.25	2.95	3.22
8		250	1			3.776	3.83	4.01	3.69
9			3			3.776	3.96	4.03	5.34
10			0.2			18.88	15.58	15.47	16.70
11		50	1			18.88	19.09	20.14	19.67
12			3			18.88	19.78	20.14	30.21
13			0.2			9.44	7.72	6.94	7.61
14	0.2	100	1	1.5D	0.5D	9.44	9.40	9.63	8.98
15			3			9.44	9.89	10.07	13.83
16			0.2			3.776	3.06	2.32	2.62
17		250	1			3.776	3.72	3.31	3.11
18			3			3.776	3.95	4.03	4.80
19			0.333			18.88	11.71	13.63	14.77
20		50	1			18.88	18.24	18.75	17.54
21			3			18.88	19.64	20.14	28.12
22			0.333			9.44	7.35	5.95	6.59
23	0.333	100	1	2.5D	D	9.44	9.03	8.32	7.85
24			3			9.44	9.80	10.07	12.65
25			0.333			3.776	2.93	1.93	2.22
26		250	1			3.776	3.56	2.74	2.65
27			3			3.776	3.90	4.03	4.30
28			0.5			18.88	14.19	12.58	13.45
29		50	1			18.88	17.54	16.57	15.65
30			3			18.88	19.60	20.14	25.89
31			0.5			9.44	6.98	5.42	5.93
32	0.5	100	1	2.5D	1.5D	9.44	8.68	7.19	6.92
33			3			9.44	9.72	10.07	11.54
34			0.5			3.776	2.83	1.73	1.97
35		250	1			3.776	3.45	2.31	2.31
36			3			3.776	3.84	4.03	3.88
37			0.75			18.88	14.53	12.31	12.61
38		50	1			18.88	16.26	14.27	13.74
39			3			18.88	19.45	20.14	23.38
40			0.75			9.44	7.46	5.27	5.52
41	0.75	100	1	2.5D	2D	9.44	8.08	6.12	6.03
42			3			9.44	9.78	10.07	10.36
43			0.75			6.293	4.82	3.18	3.38
44		150	1			6.293	5.01	3.70	3.70
45			3			6.293	6.29	6.61	6.39
46	0.95	50	1	3D	2D	18.88	14.87	12.97	12.65
47		100	1			9.44	7.54	5.55	5.53

$$SCF = \frac{2 + 2(d/D)^{3/2}(t/T)^{1/2} + 1.25(d/D)(D/T)^{1/2}}{1 + (t/T)^{3/2}(d/D)^{1/2}} \tag{6}$$

$$P^* = \frac{[A(t/T)^2 + 2289(t/T(d/D) + B\ ]\lambda + 155}{108\lambda^2 + [228(d/D)^2 + 228]\lambda + 152} \tag{7}$$

A thicker nozzle strengthens the intersection area, which leads to a higher burst pressure. This is shown in Table 5, where burst pressures derived from the finite element analysis increase with an increasing t/T and decrease with increasing D/T. The effect of different D/T, t/T, and d/D on the burst pressure is also shown in Figs. 4 and 5. Increasing the D/T, by reducing the thickness of a vessel for a fixed mean vessel diameter D, causes a lower burst pressure in a plain vessel. The impact on the burst pressure from t/T and d/D are close and significantly less than that from D/T. The burst pressures derived from FEA agree with those determined from Eqs. (4) and (5). A comparison of the burst pressure of intersections derived from FEA, and Eqs. (4) and (5) with that of plain vessels derived from the Barlow equation shows that intersections have a higher burst pressure than that of plain vessels for $t/T=3$. As a result, it can be concluded that the nozzle thickening can reinforce the cylindrical shell intersection such that its burst pressure is equal to or higher than that of the same vessel without a nozzle.

The correlation equation for burst pressure predictions is obtained by employing software package STATISTICA [17] and using the data for P_b^{FEA} given in Table 5. The result is as follows:

$$\frac{P_b}{P_{bv}} = 0.2786\left[\left(\frac{d}{D}\right)^{-0.2041} + \left(\frac{D}{T}\right)^{-0.0122} + \left(\frac{t}{T}\right)^{-0.3895}\right] \tag{8}$$

Equation (8) gives an excellent correlation, as indicated by the correlation coefficient of 0.999 and the variance of 0.9823. The residuals and percent differences between Eq. (8) and the individual FEA results are tabulated in Table 6. From this table, it is seen that the absolute percentage differences are all less than 9% except for model 19 ($d/D=0.333$, $D/T=50$, $t/T=0.333$), which has a 28.3% difference. Note that Eq. (8) has been developed

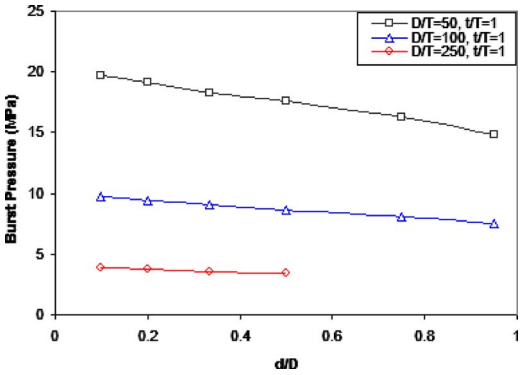

Fig. 4 Effect of D/T on the burst pressure of the cylindrical shell intersection

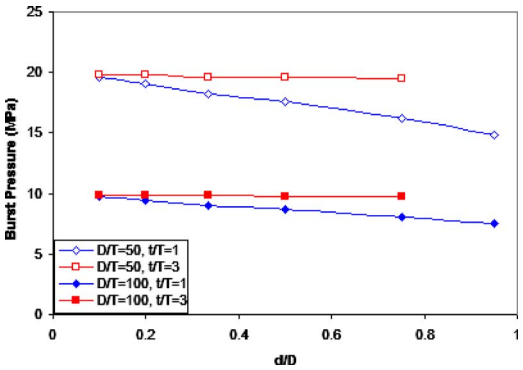

Fig. 5 Effect of t/T on the burst pressure of the cylindrical shell intersection

based on the correlations between discrete values of the geometric nondimensional parameters and burst pressures. Other biases may exist.

The FEA predicted burst pressures of the 47 models were obtained based on the material properties of carbon steel 20# (similar to A106-GrA). The correlation equation (Eq. (8)) can thus be employed to calculate the burst pressures of cylindrical shell intersections for this material. To check whether this equation can be used for other ductile metals, three materials (A672, Q235A, and 304SS) are employed to estimate the burst pressure by use of FEA for model 29 ($d/D=0.5$, $D/T=50$, $t/T=1$). The FEA material properties input (true stress-strain data) for materials A672, Q235A, and 304SS are shown in Tables 7–9, respectively. The corresponding partial stress-strain curves are shown in Figs. 6–8. The ultimate tensile strengths of A672, Q235A, and 305SS are 425 MPa, 472 MPa, and 611.3 MPa, respectively. Comparisons of the burst pressures for the three metals are given in Table 10.

Table 10 shows that the FEA predicted burst pressures using different metals are close to those calculated from the correlation equation (Eq. (8)). As a result, Eq. (8) can be used to obtain a reasonable estimate of the burst pressure for cylinder intersections of various metals. Note that different ultimate tensile strengths are incorporated in the Barlow equation (Eq. (3)) for the calculation of the burst pressure of plain vessels.

The correlation equation was developed on the basis of intersection models with $0.1 \leq d/D \leq 0.95$. Data from the three tests given in Ref. [2] and shown in Table 11 are employed to verify whether burst pressures from the tests agree with those from the correlation equation (Eq. (8)) for $d/D=1.0$ models. Note that more test data are given in Ref. [2] for $D/T<50$. It is seen that the percentage differences in the predictions of the test data and the equation are less than 13%. Therefore, Eq. (8) can be extrapolated for use at $d/D=1.0$.

In summary, the correlation equation (Eq. (8)) has been shown to be applicable for the following ranges of geometric parameters of cylindrical shell intersections:

$$0.1 \leq d/D \leq 1.0$$

Table 6 Comparison of Eq. (8) with FEA results

Model	d/D	D/T	t/T	P_b^{FEA}	$P_b^{Eq.\ (8)}$	Residual	Diff. (%)
1	0.1	50	0.1	15.81	15.58	0.23	1.5
2	0.1	50	1	19.65	18.69	0.96	4.9
3	0.1	50	3	19.78	21.50	−1.72	−8.7
4	0.1	100	0.1	8.16	7.77	0.39	4.8
5	0.1	100	1	9.72	9.32	0.40	4.1
6	0.1	100	3	9.87	10.73	−0.86	−8.7
7	0.1	250	0.1	3.25	3.10	0.15	4.7
8	0.1	250	1	3.83	3.72	0.11	2.9
9	0.1	250	3	3.96	4.28	−0.32	−8.1
10	0.2	50	0.2	15.58	15.13	0.45	2.9
11	0.2	50	1	19.09	17.58	1.51	7.9
12	0.2	50	3	19.78	20.39	−0.61	−3.1
13	0.2	100	0.2	7.72	7.54	0.18	2.3
14	0.2	100	1	9.40	8.77	0.63	6.7
15	0.2	100	3	9.89	10.17	−0.28	−2.9
16	0.2	250	0.2	3.06	3.01	0.05	1.7
17	0.2	250	1	3.72	3.50	0.22	6.0
18	0.2	250	3	3.95	4.06	−0.11	−2.8
19	0.333	50	0.333	11.71	15.03	−3.32	−28.3
20	0.333	50	1	18.24	16.86	1.38	7.6
21	0.333	50	3	19.64	19.67	−0.03	−0.1
22	0.333	100	0.333	7.35	7.49	−0.14	−1.9
23	0.333	100	1	9.03	8.41	0.62	6.9
24	0.333	100	3	9.80	9.81	−0.01	−0.1
25	0.333	250	0.333	2.93	2.99	−0.06	−1.9
26	0.333	250	1	3.56	3.35	0.21	5.8
27	0.333	250	3	3.90	3.91	−0.01	−0.4
28	0.5	50	0.5	14.19	15.09	−0.90	−6.3
29	0.5	50	1	17.54	16.34	1.20	6.9
30	0.5	50	3	19.60	19.14	0.46	2.3
31	0.5	100	0.5	6.98	7.52	−0.54	−7.8
32	0.5	100	1	8.68	8.15	0.53	6.1
33	0.5	100	3	9.72	9.55	0.17	1.7
34	0.5	250	0.5	2.83	3.00	−0.17	−6.0
35	0.5	250	1	3.45	3.25	0.20	5.9
36	0.5	250	3	3.84	3.81	0.03	0.8
37	0.75	50	0.75	14.53	15.30	−0.77	−5.3
38	0.75	50	1	16.26	15.85	0.41	2.5
39	0.75	50	3	19.45	18.66	0.79	4.0
40	0.75	100	0.75	7.46	7.63	−0.17	−2.2
41	0.75	100	1	8.08	7.91	0.17	2.2
42	0.75	100	3	9.78	9.31	0.47	4.8
43	0.75	150	0.75	4.82	5.08	−0.26	−5.3
44	0.75	150	1	5.01	5.26	−0.25	−5.0
45	0.75	150	3	6.29	6.20	0.09	1.5
46	0.95	50	1	14.87	15.59	−0.72	−4.8
47	0.95	100	1	7.54	7.77	−0.23	−3.1

Table 7 Multilinear material model for material A672

Points	1	2	3	4	5	6	7	8	9	10	11
Strain ($\mu\varepsilon$)	1544	5983	13,700	21,400	49,000	81,800	113,900	167,600	196,800	220,200	245,000
Stress (MPa)	295	296.83	317.18	333.05	389.37	434.33	465.33	503	519.11	529.75	537.88

Table 8 Multilinear material model for material Q235A

Points	1	2	3	4	5	6	7	8
Strain ($\mu\varepsilon$)	1250	3135	17,250	28,976	38,644	67,098	94,765	130,502
Stress (MPa)	251	340.47	345.31	374.29	429.58	486.79	522.43	552.50

Table 9 Multilinear material model for material 304SS

Points	1	2	3	4	5	6	7	8	9
Strain ($\mu\varepsilon$)	1609	26,886	64,401	99,098	166,445	208,947	249,717	307,915	344,913
Stress (MPa)	322.5	390.0	456.0	509.4	601.5	662.2	715.4	806.3	863.1

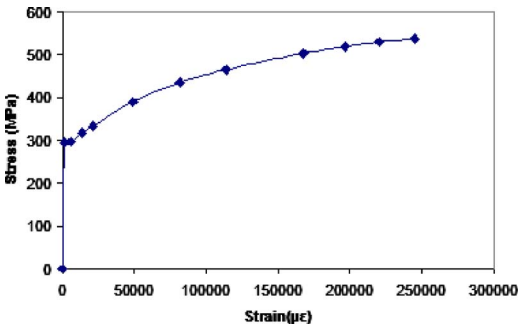

Fig. 6 Stress-strain curve of material A672

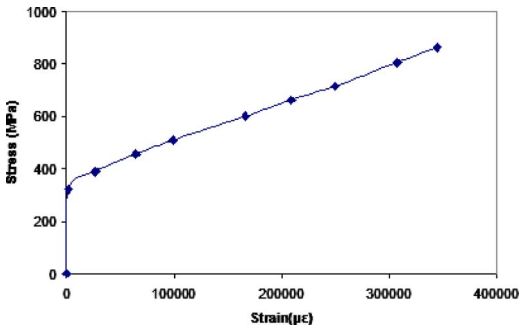

Fig. 8 Stress-strain curve of material 304SS

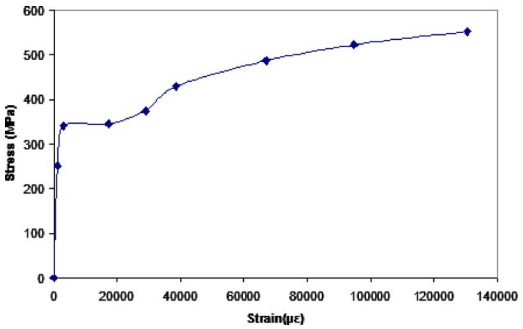

Fig. 7 Stress-strain curve of material Q235A

Table 10 Burst pressure comparison of different metals for model 29 ($d/D=0.5$, $D/T=50$, $t/T=1$)

Material	σ_u (MPa)	P_b^{FEA} (MPa)	$P_b^{Eq.\ (8)}$ (MPa)	Diff. (%)
A672	425	15.92	14.71	7.60
Q235A	472	17.58	16.33	7.11
304SS	611.3	20.11	21.15	−5.17

$$50 \leq D/T \leq 150$$

$$d/D \leq t/T \leq 3.0$$

7 Conclusions

Based on a validation of the nonlinear FEA procedure [12], a parametric analysis has been carried out to determine the burst pressures of radial cylindrical shell intersections using the arc length method. A correlation equation (Eq. (8)) was developed. From the results obtained, the following conclusions can be reached:

1. A nonlinear finite element simulation along with the arc length method can be employed to predict the burst pressure of cylinder-cylinder intersections.
2. The failure can be estimated based on the value of the maximum of the average equivalent plastic strain across the thickness at various cross sections.
3. Equation (8) can be employed to estimate the burst pressures of cylindrical shell intersections.
4. The geometric parameters d/D, D/T, and t/T affect the burst pressure of cylindrical shell intersections. The burst pressure increases with t/T and decreases with D/T. The effects of d/D and t/T are less striking when compared with D/T.

Table 11 Burst pressure comparison for $d/D=1.0$ models

D_o (in.)	T (in.)	d_o (in.)	t (in.)	d/D	D/T	t/T	σ_u (psi)	$P_b^{Ref.\ [3]}$ (psi)	$P_b^{Eq.8}$ (psi)	Diff. (%)
8.625	0.50	8.625	0.50	1	16.25	1	58,650	6400[a]	5966	6.78
24.00	0.312	24.00	0.312	1	75.92	1	84,300	1620	1824	−12.61
4.50	0.237	4.50	0.237	1	17.99	1	69,000	5750[a]	6338	−10.23

[a]Average of test data. 1 in.=25.4 mm.

Nomenclature

D = mean diameter of the vessel
D_i = inside diameter of the vessel
E = Young's modulus
L_a = length of the vessel
L_n = length of the nozzle
L_v = half-length of the vessel
P_b = burst pressure of the cylindrical shell intersection
P_{bv} = burst pressure of the plain vessel
T = wall thickness of the vessel
d = mean diameter of the nozzle
d_i = inside diameter of the nozzle
t = wall thickness of the nozzle
σ_u = ultimate tensile strength
σ_y = yield strength

References

[1] Cottam, W. J., and Gill, S. S., 1966, "Experimental Investigation of the Behavior Beyond the Elastic Limit of Flush Nozzle in Cylindrical Pressure Vessels," J. Mech. Eng. Sci., **8**(3), pp. 330–354.

[2] Rodabaugh, E. C., 1988, "A Review of Area Replacement Rules for Pipe Connections in Pressure Vessels and Piping," Weld. Res. Counc. Bull. No. 335.

[3] Sang, Z. F., Xue, L., Lin, Y., and Widera, G. E. O., 2000, "Limit Analysis and Burst Test for Large Diameter Intersections," Weld. Res. Counc. Bull., No. 451.

[4] Jones, D. P., Holliday, J. E. and Larson, L. D., 1999, "Elastic-Plastic Failure Analysis of Pressure Burst Tests of Thin Toroidal Shells," ASME J. Pressure Vessel Technol., **121**, pp. 149–153.

[5] Jones, D. P., and Holliday, J. E., 2000, "Elastic-Plastic Analysis of the PVRC Burst Disk Tests With Comparison to the ASME Code Primary Stress Limits," ASME J. Pressure Vessel Technol., **122**, pp. 146–151.

[6] Kisioglu, Y., Brevick, I. R., and Kinzel, G. L., 2001, "Determinations of Burst Pressure and Location of the DOT-39 Refrigerant Cylinders," ASME J. Pressure Vessel Technol., **123**, pp. 240–247.

[7] Lourerio, J. F., Netto, T. A., and Estefen, S. F., 2001, "On the Effect of Corrosion Defects in the Burst Pressure of Pipelines," *Proceedings of the 20th International Conference on Offshore Mechanics and Arctic Engineering*, Rio de Janeiro, Brazil, Paper No. OMAE2001/PIPE-4103.

[8] Chouchaoui, B. A., Pick, R. J., and Yost, D. B., 1992, "Burst Pressure Prediction of Line Pipe Containing Single Corrosion Pits Using Finite Element Method," *Proceedings of the International Conference on Offshore Mechanics and Arctic Engineering (OMAE)*, Volume 5A, ASME, New York.

[9] Błachut, J., and Vu, V. T., 2007, "Burst Pressures for Torispheres and Shallow Spherical Caps," Strain, **43**, pp. 26–36.

[10] Cronin, D. S., 2002, "Finite Element Analysis of Complex Corrosion Defects," *Pressure Vessel and Piping, Computational Mechanics: Developments and Applications*, **441**, pp. 55–61.

[11] Xue, L., 2006, "Elastic and Inelastic Finite Element Analysis of Cylindrical Shell Intersections," Ph.D. thesis, Marquette University, Milwaukee, WI.

[12] Wang, H. F., Sang, A. F., Xue, L. P., and Widera, G. E. O., 2009, "Burst Pressure of Pressurized Cylinders With the Hillside Nozzle," ASME J. Pressure Vessel Technol., **131**(4), p. 041204.

[13] Swanson Analysis System Inc., 2003, Analysis Engineering Analysis Systems User's Manual.

[14] Widera, G. E. O., and Xue, L., 2004, "Guidelines for Modeling Cylinder-to-Cylinder Intersections," Weld. Res. Counc. Bull., No. 493.

[15] Widera, G. E. O., and Wei, Z., 1997, "Parametric Finite Element," PVRC, Report No. 95-15.

[16] Widera, G. E. O., and Wei, Z., 1998, "Parametric Finite Element Analysis of Large Diameter Shell Intersections, Part 2. External Loadings," PVRC, Project Report No. 96-20AS.

[17] Statsoft Inc., 1993, STATISTICA for Windows Release 4.5.